

# LI-RADS for CT diagnosis of hepatocellular carcinoma: performance of major and ancillary features

Ayman Alhasan,<sup>1,2</sup> Milena Cerny,<sup>3</sup> Damien Olivie,<sup>1</sup> Jean-Sébastien Billiard,<sup>1</sup> Catherine Bergeron,<sup>1</sup> Kip Brown,<sup>3</sup> Paule Bodson-Clermont,<sup>3</sup> Hélène Castel,<sup>4</sup> Simon Turcotte,<sup>3,5</sup> Pierre Perreault,<sup>1</sup> and An Tang<sup>1,3,6</sup>

<sup>1</sup>Department of Radiology, Centre Hospitalier de l'Université de Montréal (CHUM), Montreal, QC H2X 0C2, Canada

<sup>2</sup>Faculty of Medicine, Taibah University, Medina, Saudi Arabia

<sup>3</sup>Centre de Recherche du Centre Hospitalier de l'Université de Montréal (CRCHUM), 900, rue Saint-Denis (Tour Viger), Montreal, QC H2X 0A9, Canada

<sup>4</sup>Department of Hepatology and Liver Transplantation, Centre Hospitalier de l'Université de Montréal (CHUM), Montreal, QC, Canada

<sup>5</sup>Department of Surgery, Hepatopancreatobiliary and Liver Transplantation Service, Centre Hospitalier de l'Université de Montréal (CHUM), Montreal, QC, Canada

<sup>6</sup>Department of Radiology, Radio-Oncology and Nuclear Medicine, University of Montreal, Montreal, QC, Canada

## Abstract

**Purpose:** To evaluate the diagnostic performance of Liver Imaging Reporting and Data System (LI-RADS) v2017 major features, the impact of ancillary features, and categories on contrast-enhanced computed tomography (CECT) for the diagnosis of hepatocellular carcinoma (HCC).

**Materials and methods:** This retrospective study included 59 patients (104 observations including 72 HCCs) with clinical suspicion of HCC undergoing CECT between 2013 and 2016. Two radiologists independently assessed major and ancillary imaging features for each liver observation and assigned a LI-RADS category based on major features only and in combination with ancillary features. The composite reference standard included pathology or imaging. Per-lesion estimates of diagnostic performance of major features, ancillary features, and LI-RADS categories were assessed by generalized estimating equation models.

**Results:** Major features (arterial phase hyperenhancement, washout, capsule, and threshold growth) respectively had a

sensitivity of 86.1%, 81.6%, 20.7%, and 26.1% and specificity of 39.3%, 67.9%, 89.9%, and 85.0% for HCC. Ancillary features (ultrasound visibility as discrete nodule, subthreshold growth, and fat in mass more than adjacent liver) respectively had a sensitivity of 42.6%, 50.8%, and 15.1% and a specificity of 79.2%, 66.9%, and 96.4% for HCC. Ancillary features modified the final category in 4 of 104 observations. For HCC diagnosis, categories LR-3, LR-4, LR-5, and LR-TIV (tumor in vein) had a sensitivity of 5.3%, 29.0%, 53.7%, and 10.7%; and a specificity of 49.1%, 84.4%, 97.3%, and 96.4%, respectively.

**Conclusion:** On CT, LR-5 category has near-perfect specificity for the diagnosis of HCC and ancillary features modifies the final category in few observations.

**Key words:** LI-RADS—Hepatocellular carcinoma—Major features—Ancillary features—Category—CT

Hepatocellular carcinoma (HCC) is the most common primary malignant tumor of the liver, the fifth and seventh most common cancer in men and women, respectively. It is the second leading cause of deaths related to cancer worldwide [1].

**Electronic supplementary material** The online version of this article (<https://doi.org/10.1007/s00261-018-1762-2>) contains supplementary material, which is available to authorized users.

Correspondence to: An Tang; email: an.tang@umontreal.ca

Unlike many other cancers, under certain conditions HCC can be diagnosed with imaging, without the need for pathology confirmation in many cases. Several diagnostic systems advocate using contrast-enhanced ultrasound, computed tomography (CT) or magnetic resonance imaging (MRI) for the non-invasive diagnosis of HCC [2–5]. The Liver Imaging Reporting and Data System (LI-RADS) has been developed for the standardized interpretation, reporting, and data collection of liver imaging examinations in patients at risk for HCC [3, 6]. LI-RADS assigns categories to liver observations that reflect their probability of HCC. The development of LI-RADS is based on a combination of evidence, expert opinion, and the desire to maintain congruency with American Association for the Study of Liver Diseases (AASLD) and United Network for Organ Sharing-Organ Procurement and Transplantation Network (UNOS-OPTN) guidelines [4, 7, 8]. However, there is a need to validate the diagnostic performance of LI-RADS categories, major and ancillary imaging features. Prior studies have focused on the reproducibility of LI-RADS categories and major features [9–11]. Some studies have reported the diagnostic performance of LI-RADS categories [10–13], major features [12, 13], and ancillary features [11–13] in earlier versions (2011 or 2014).

LI-RADS has been updated in 2017 based on evidence from recent studies [3], expert consensus and multidisciplinary feedback. The 2017 version includes revised categories, explicit criteria for LR-M, updated definitions and clarifications on the use of ancillary features. LI-RADS is presently the only diagnostic system that allows the use of ancillary features to adjust the probability of HCC. Some of these ancillary features favor malignancy in general, some favor HCC in particular, and others favor benignity. Radiologists can choose to apply ancillary features to readjust the category by upgrading or downgrading the LI-RADS category initially assigned based on major features only. CT, MRI, and contrast-enhanced ultrasound may be used for diagnosis of HCC and categorization of liver observations using major and ancillary features. CT scans are widely available, less prone to artifacts, less time consuming, have a lower cost, and also require less experience for interpretation compared to MRI [14]. High spatial resolution and isotropic acquisitions are suitable for multiplanar reconstructions [15]. For evaluation of focal liver lesions, CT has a sensitivity and specificity similar to that of MRI according to recent meta-analyses [16, 17].

Therefore, the primary purpose of this study was to evaluate the diagnostic performance of LI-RADS version 2017 major features, ancillary features, and categories on CT for the diagnosis of HCC. The secondary purpose was to evaluate the interreader agreement.

## Materials and methods

### *Study design and subjects*

This retrospective, cross-sectional, single-site study was approved by the institutional review board at the Centre Hospitalier de l'Université de Montréal (CHUM). Patient consent was waived. The study flowchart is illustrated in Fig. 1. All eligible patients were identified using the inclusion and exclusion criteria listed in Table 1.

### *Characteristics of patients and observations*

Between January 2013 and September 2016, 59 patients (104 observations including 72 HCCs) met the inclusion criteria. Characteristics of patients, observations, LR categories, final diagnosis, and time interval between index CT imaging and reference standards are summarized in Table 2. In our study, the mean diameter for all observations was  $30.1 \text{ mm} \pm 23.4$  (range, 6–110 mm). The mean diameter of HCCs evaluated was  $34.4 \text{ mm} \pm 23.4$  (range, 9–110 mm). Our study included a total of 104 observations. The average number of observations per patient was  $1.8 \pm 1.3$  (range, 1–10).

### *CT imaging protocols*

All CT scans were performed with various multidetector CT (MDCT) scanners available at our institution (16 and 64 MDCT scanners). An unenhanced phase—which is optional according to the LI-RADS technical recommendations—was performed in some patients. All CT examinations included at least three vascular phases covering the upper abdomen CT technique. Details of the CT protocol are provided in Supplementary Table 1.

### *Observation registry*

The CT performed for characterization of one or more observation was chosen as the index test. One reader (A.A., 9 years of experience in radiology) and reported diameter and location according to Couinaud classification of liver segments for each observation (1–10 maximum per patient) and provided a list for review. The previous examination (ultrasound, CT, or MRI) was used to evaluate for visibility as discrete nodule and growth when applicable.

### *CT review*

Two senior abdominal radiologists with experience in liver imaging (D.O. and J.S.B., with 21 and 23 years of experience, respectively) independently reviewed all the CT examinations on picture archiving and communication system workstations (Impax version 6.6, Agfa HealthCare, Mortsel, Belgium) using the size and local-

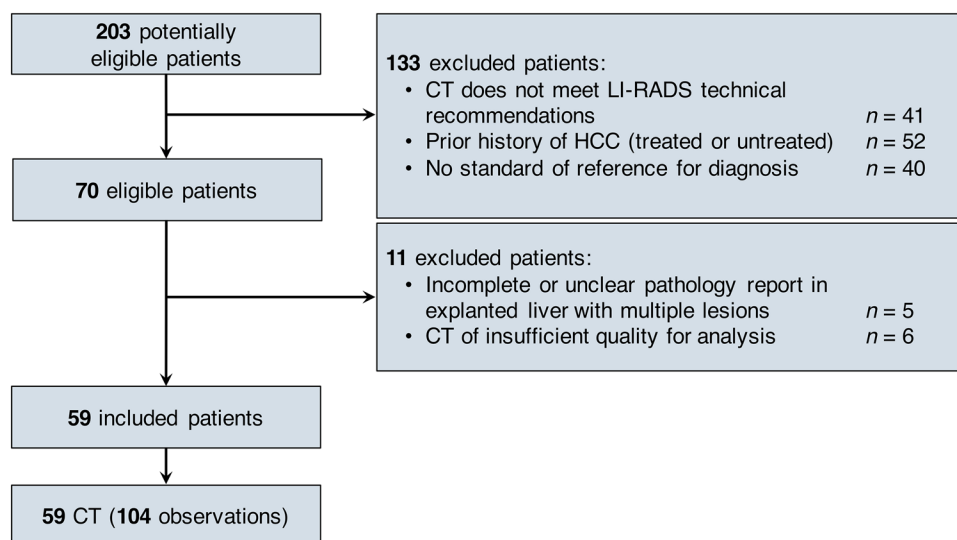


Fig. 1. Flowchart of patient selection. *HCC* hepatocellular carcinoma.

Table 1. Inclusion and exclusion criteria

#### Inclusion criteria

1. Clinical suspicion of HCC between January 2013 and September 2016
2. The 3- or 4-phase contrast-enhanced CT (CECT) met the LI-RADS v2017 technical recommendations
3. The CECT was performed at our tertiary care referral center
4. There was at least one lesion proven by pathology per patient or follow-up imaging demonstrating significant growth, typical features of HCC or lipiodol accumulation after hepatic arterial chemoembolization

#### Exclusion criteria

1. Subjects had a prior history of HCC (treated or untreated)
2. The CT quality was sub-optimal or inadequate for diagnostic evaluation
3. CT was performed without intravenous contrast or did not meet LI-RADS technical recommendations
4. There was no pathology result or follow-up imaging at least 6 months after initial CT
5. Incomplete or unclear pathology reports in explanted livers with multiple liver lesions

*HCC* hepatocellular carcinoma; *LI-RADS* liver imaging reporting and data system

ization of observations as a guide. There were no annotations or measurements on images at the time of review. Information about observations' growth or ultrasound visibility as discrete nodule was provided to the reviewers at the time of review. Assessment of major and ancillary features was conducted according to the LI-RADS version 2017 [3]. Images were bookmarked by the author and used as a guide.

### Blinding

Both readers were aware of the design and purpose of the study, but were blinded to the clinical history, imaging report, and final diagnosis.

### Image analysis

Each reader independently assessed each major and ancillary features for all bookmarked observations, except for diameter, threshold growth, ultrasound visibility as discrete nodule, and subthreshold growth which were

assessed by the reader (A.A., 9 years of experience in radiology) who bookmarked all observations.

Each reader separately assigned a LI-RADS category that reflects the probability of HCC: LR-NC for observations that cannot be categorized due to image degradation or omission, LR-1 for definitely benign, LR-2 for probably benign, LR-3 for intermediate probability of HCC, LR-4 for probably HCC, LR-5 for definitely HCC, LR-TIV for tumor in vein, and LR-M for probably or definitely malignant but not specific for HCC [3]. Categorization was performed in two steps process: first, using LI-RADS major imaging features only; then, after evaluation and application of ancillary features. When a feature could not be assessed (for example: blood products in mass cannot be evaluated in a patient without an unenhanced phase) then it was considered as non-applicable. Each reader was given the choice to adjust (upgrade or downgrade) the final category for each observation based on the presence of ancillary features. Readers were not allowed to upgrade from LR-4 to LR-5 category as defined by LI-RADS. Disagreements on major features, ancillary features, and LI-RADS cate-

**Table 2.** Characteristics of patients, observations, reference standards, and index tests included in study cohort

Characteristic	Data
Patients	
Sex	
Male	45/59 (76.3)
Female	14/59 (23.7)
Age (year)	
Mean $\pm$ standard deviation	63.2 $\pm$ 10.7
At least one HCC	54/59 (91.5)
Known cirrhosis	55/59 (93.2)
Etiology of liver disease	
Hepatitis C infection	17/59 (28.8)
Hepatitis B infection	3/59 (5.1)
Alcoholic liver disease	12/59 (20.3)
Non-alcoholic steatohepatitis	10/59 (17.0)
Primary biliary cirrhosis	1/59 (1.7)
Autoimmune hepatitis	2/59 (3.4)
Hemochromatosis	3/59 (5.1)
Other causes	11/59 (18.6)
Observations	
Observation size (mm)	
Mean $\pm$ standard deviation	30.1 $\pm$ 23.4
Range	6–110
HCC size (mm)	
Mean $\pm$ standard deviation	34.4 $\pm$ 23.4
Range	9–110
Stratified according to size thresholds	
< 10 mm	5/104 (4.8)
10–19 mm	41/104 (39.4)
$\geq$ 20 mm	58/104 (55.8)
Categorization according to major features only (LI-RADS v2017)	
LR-1	1/104 (1.0)
LR-2	3/104 (2.9)
LR-3	19/104 (18.3)
LR-4	27/104 (26.0)
LR-5	42/104 (40.3)
LR-TIV	9/104 (8.6)
LR-M	3/104 (2.9)
Categorization after application of ancillary features	
LR-1	1/104 (1.0)
LR-2	5/104 (4.8)
LR-3	15/104 (14.4)
LR-4	29/104 (27.9)
LR-5	42/104 (40.4)
LR-TIV	9/104 (8.6)
LR-M	3/104 (2.9)
Index tests	
Time interval between index CT imaging and pathological analysis as reference standard (days)	
For HCC	
Mean $\pm$ standard deviation	137 $\pm$ 206
Range	0–932
For benign entities:	
Mean $\pm$ standard deviation	251 $\pm$ 441
Range	8–904
Time interval between index CT imaging and imaging as reference standard (days)	
For HCC	
Mean $\pm$ standard deviation	227 $\pm$ 248
Range	0–791
For benign entities	
Mean $\pm$ standard deviation	150 $\pm$ 87
Range	0–256
Reference standards	
Pathological analysis	43/104 (41.3)
Follow-up imaging	61/104 (58.7)
Final diagnosis	
HCC	72/104 (69.2)
Cholangiocarcinoma	3/104 (2.8)

**Table 2.** continued

Characteristic	Data
Dysplastic nodules	2/104 (1.9)
Adenoma	1/104 (1.0)
Cysts	3/104 (2.9)
Hemangioma	6/104 (5.8)
Perfusional alteration	1/104 (1.0)
Neuroendocrine tumor	1/104 (1.0)
Others (confluent fibrosis, focal scar and focal cirrhosis)	15/104 (14.4)

Unless specified, data are numerators and denominators, and data in parentheses are percentages

HCC hepatocellular carcinoma, LI-RADS Liver Imaging Reporting and Data System

gories were solved by consensus at least 2 weeks after the initial interpretation.

### Reference standard

The unit of analysis was per lesion. A composite reference standard was established based on (a) histopathological confirmation for 43 observations, including image-guided biopsy specimen ( $n = 16$ ), hepatectomy ( $n = 14$ ), and explant ( $n = 13$ ); (b) imaging for 61 observations, including follow-up imaging demonstrating significant growth ( $\geq 50\%$  diameter increase in less than 6 months or  $\geq 100\%$  diameter increase in more than 6 months), recurrence after local treatment or new lesion demonstrated by MRI ( $n = 52$ ), CT ( $n = 3$ ), contrast-enhanced ultrasound (CEUS) ( $n = 2$ ), MRI demonstrating typical features of HCC, or ethiodized oil (lipiodol; Lipiodol Ultra-fluid, Guerbet, Villepinte, France) fixation within the tumor ( $n = 4$ ). The assessor of the reference standard (A.A., 9 years of experience in radiology) had access to clinical history, index and previous imaging, and pathological information but did not participate in the assessment of the index test. Since non-malignant lesions are rarely assessed by pathological analysis, the reference standards for LR-1, and LR-2 observations were based on typical imaging findings on another imaging modality or the absence of progression to a higher category (LR-4, LR-5) during the follow-up. The reference standard for LR-3 observations was follow-up imaging except when pathology was available.

### Statistical analysis

Statistical analyses were supervised by a biostatistician (P.B.C., 7 years of experience) and performed by a data scientist (K.B., 8 years of experience) with statistical software (SAS version 9.4; SAS Institute Inc., Cary, NC). Continuous variables were expressed as mean  $\pm$  standard deviation (SD), minimum and maximum. Categorical variables were expressed as numbers and percentages.

*Diagnostic performance of imaging features.*—Estimates of diagnostic performance (including sensitivity, specificity, accuracy, positive predictive value, negative predictive value) of major and ancillary features were calculated separately for each reader (R1 and R2) and also for the consensus interpretation. A generalized estimating equation (GEE) model based on a binomial distribution with an identity link function and an exchangeable correlation matrix was used to compute estimates of diagnostic performance while taking into account patient cluster effect due to the presence of several observations in the same patients. Diagnostic odds ratios were computed by using a GEE model based on a binomial distribution with a logit link function and an exchangeable correlation matrix. The point estimates and 95% confidence (CI) intervals were reported.

*Diagnostic performance of LI-RADS categories.*—The diagnostic performance of LI-RADS categories was reported for each category before and after applying ancillary features. The diagnostic performance was also reported for the following combinations (LR-5 + LR-TIV) and (LR-4, LR-5 + LR-TIV) before and after applying ancillary features. The diagnostic performance was calculated for each reader separately (R1 and R2) and also for the consensus interpretation. Similarly, GEE models were used to account for patient cluster effect during computation of point estimates and 95% CI.

*Impact of ancillary features.*—The number of observations in which ancillary features upgraded or downgraded the final LI-RADS category was documented.

*Interreader agreement.*—Cohen's kappa with 95% confidence intervals was used to determine interreader agreement. The 95% bias-corrected bootstrap confidence intervals using 1000 bootstrap samples were computed. Agreement was interpreted as slight (0.01–0.20), fair (0.21–0.40), moderate (0.41–0.60), substantial (0.61–0.80), or almost perfect (0.81–1.00) [18]. Considering the observed marginal distribution, the inter-reader agreement for major features, ancillary features, LI-RADS categories according to major features only and combination of major and ancillary features were documented also with proportion of agreement. Inter-reader agreement could not be computed for some features because of their low frequency.

## Results

### *Diagnostic performance of major features*

Table 3 summarizes the per-lesion diagnostic performance of major features. Sensitivity of major features for HCC ranged from 20.7% to 86.0% for consensus. Diameter threshold had the highest sensitivity of 98.7% followed by arterial phase hyperenhancement. Capsule appearance had the lowest sensitivity. Specificity ranged from 39.9% to 89.9% and was highest for enhancing capsule. Observation size more than 10 mm had the

lowest specificity of 1.3%. Positive predictive value ranged from 50.0% to 90.5% and was highest for wash-out. Figure 2 illustrates an example of HCC diagnosed based on major features.

### *Diagnostic performance of ancillary features*

Table 4 summarizes the per-lesion diagnostic performance of ancillary features favoring malignancy in general or HCC in particular. Sensitivity ranged from 1.3% to 50.8% and was highest for subthreshold growth. Specificity ranged from 66.9% to 96.4% and was highest for fat in mass more than adjacent liver. Positive predictive value ranged from 78.4% to 90.3% and was highest for fat in mass more than surrounding liver. Figure 3 illustrates an example of an HCC diagnosed based on major features in combination with ancillary features.

### *Diagnostic performance of LI-RADS categories*

The diagnostic performances of LI-RADS categories before and after applying ancillary features are summarized in Supplementary Tables 2 and 3. The sensitivity of LR-5 or LR-TIV was 65.5%. The sensitivity of the combination of LR-4, LR-5, or LR-TIV was 94.7% with major features only and 96% according to major and ancillary features. The specificity of LR-5 or LR-TIV was 91.3%. The specificity of LR-4, LR-5, or LR-TIV was 75.2% with major features only and 71.3% according to major and ancillary features. Figure 4 illustrates the proportion of HCC for each LI-RADS category.

### *Ancillary features impact on observation categories*

The numbers and percentages of observation categories before and after application of ancillary features are illustrated in Figure 5. The observation category before and after applying ancillary features was identical in 96.2% of observations (100 of 104). When taking into account the rules determined by LI-RADS v2017, ancillary features modified the category in 3.8% of all observations (4 of 104). The observation category was upgraded in 8.7% (2 of 23 observations eligible for category upgrade) and downgraded in 4.1% (2 of 49 observations eligible for category downgrade). The two observations categorized LR-3 based on major features and upgraded to LR-4 based on ancillary features were a 10-mm HCC with subthreshold growth and a 16-mm hemangioma with suspicion of intra-lesional fat. The two observations categorized LR-3 based on major features and downgraded to LR-2 based on ancillary features were two 11-mm hemangiomas that had enhancement that paralleled blood pool.

**Table 3.** Per-lesion diagnostic performance of major features according to LI-RADS v2017 algorithm

Major features	No. of observations			Sensitivity (%)	Specificity (%)	Accuracy (%)	Positive predictive value (%)	Negative predictive value (%)	Diagnostic odds ratio
	TP	FN	TN						
<b>Diameter threshold ≥ 10 mm</b>									
Reader 1	-	-	-	-	-	-	-	-	-
Reader 2	-	-	-	-	-	-	-	-	-
Bookmarked	74	1	25	98.7 (96.0–101.3)	13.5 (0.0–27.4)	78.7(70.3–87.2)	79.1 (70.4–87.7)	78.4 (39.7–117.0)	9.05 (1.90–43.19)
<b>Diameter threshold ≥ 20 mm</b>									
Reader 1	-	-	-	-	-	-	-	-	-
Reader 2	-	-	-	-	-	-	-	-	-
Bookmarked	51	24	7	65.4 (53.7–77.2)	75.9 (61.2–90.6)	69.7 (62.4–77.0)	88.3 (80.1–96.5)	40.5 (24.6–56.3)	6.28 (2.36–16.75)
<b>Arterial phase hyperenhancement</b>									
Reader 1	65	10	17	86.0 (77.8–94.2)	40.8 (20.7–60.8)	74.2 (65.5–82.9)	82.9 (74.3–91.4)	50.0 (28.1–71.9)	5.30 (1.86–15.09)
Reader 2	65	10	18	86.0 (77.8–94.2)	35.8 (16.4–55.3)	73.3 (64.4–82.3)	81.6 (72.9–90.2)	44.4 (21.5–67.4)	3.75 (1.20–11.71)
Consensus	65	10	17	86.0 (77.8–94.2)	39.3 (18.3–60.3)	74.4 (65.4–83.3)	83.1 (74.8–91.4)	44.4 (21.5–67.4)	4.57 (1.38–15.09)
<b>Washout</b>									
Reader 1	61	14	9	83.1 (74.1–92.1)	67.9 (47.5–88.3)	78.8 (70.4–87.1)	90.6 (83.1–98.0)	57.6 (39.6–75.6)	11.10 (3.82–32.29)
Reader 2	62	13	9	81.6 (72.6–90.7)	67.9 (47.5–88.3)	77.7 (69.2–86.1)	90.5 (83–98.0)	55.0 (36.7–73.3)	10.49 (3.64–30.26)
Consensus	61	14	9	81.6 (72.6–90.7)	67.9 (47.5–88.3)	77.7 (69.2–86.1)	90.5 (83–98.0)	55.0 (36.7–73.3)	10.49 (3.64–30.26)
<b>Arterial phase hyperenhancement and washout</b>									
Reader 1	52	23	6	68.9 (58.1–79.7)	70.7 (57.5–84.0)	72.1 (64.3–79.8)	90.3 (82.6–98)	46.6 (31.4–61.8)	8.25 (2.77–24.58)
Reader 2	51	24	6	67.8 (57.1–78.5)	75.8 (61.1–90.5)	70.7 (62.2–79.3)	90.0 (82.3–97.7)	42.3 (26.6–57.9)	7.74 (2.52–23.78)
Consensus	51	24	6	67.8 (57.1–78.5)	75.8 (61.1–90.5)	70.7 (62.2–79.3)	90.0 (82.3–97.7)	42.3 (26.6–57.9)	7.74 (2.52–23.78)
<b>Enhancing “capsule”</b>									
Reader 1	22	53	2	26.8 (20.6–33.1)	87.9 (78.8–97.0)	45.9 (36.1–55.7)	50.0 (50.0–50.1)	29.1 (17.9–40.2)	6.09 (1.10–33.58)
Reader 2	14	61	1	18.2 (10.2–26.1)	89.9 (79.8–100.1)	38.4 (28.4–48.4)	50.0 (50.0–50.1)	27.7 (17.5–37.9)	7.85 (0.54–113.96)
Consensus	16	59	1	20.7 (12.2–29.1)	89.9 (79.8–100.1)	40.7 (30.7–50.7)	50.0 (50.0–50.1)	28.6 (18.1–39.0)	8.57 (0.65–113.23)
<b>Threshold growth</b>									
Reader 1	-	-	-	-	-	-	-	-	-
Reader 2	-	-	-	-	-	-	-	-	-
Bookmarked	13	37	4	26.1 (12.7–39.5)	85.0 (66.4–103.7)	40.5 (27.8–53.2)	85.4 (66.7–104.1)	26.7 (13.6–39.8)	1.01 (0.20–5.19)

Data in parentheses are 95% confidence intervals. Estimates of diagnostic performance were calculated with a generalized estimating equation (GEE) model to account for patient cluster effect. Dashes indicate that imaging feature was not evaluated by readers or that estimates of diagnostic performance could not be computed with GEE model because of small number of observations displaying this ancillary feature. Observation diameters and threshold growth were based on bookmarked measurements  
*FN* false-negative; *FP* false-positive; *TN* true-negative; *TP* true-positive

**Table 4.** Per-lesion diagnostic performance of ancillary features in favor of malignancy in general and hcc in particular

Ancillary features	No. of observations				Sensitivity (%)	Specificity (%)	Accuracy (%)	Positive predictive value (%)	Negative predictive value (%)	Diagnostic odds ratio
	TP	FN	FP	TN						
US visibility as discrete nodule										
Reader 1	-	-	-	-	-	-	-	-	-	-
Reader 2	-	-	-	-	-	-	-	-	-	-
Bookmarked	23	32	4	16	42.6 (27.7–57.6)	79.2 (60.8–97.6)	51.7 (39.1–64.3)	85.5 (72.6–98.4)	31.4 (16.9–45.9)	2.64 (0.70–9.88)
Subthreshold growth										
Reader 1	-	-	-	-	-	-	-	-	-	-
Reader 2	-	-	-	-	-	-	-	-	-	-
Bookmarked	25	25	5	12	50.8 (36.1–65.5)	66.9 (40.3–93.5)	55.0 (42.4–67.6)	86.5 (73.9–99.0)	28.1 (12.2–43.9)	2.40 (0.58–9.86)
Corona enhancement										
Reader 1	2	73	1	28	-	-	-	-	-	-
Reader 2	3	72	1	28	-	-	-	-	-	-
Consensus	4	71	1	28	-	-	-	-	-	-
Fat sparing in solid mass										
Reader 1	0	61	0	25	-	-	23.0 (13.1–32.9)	-	23.0 (13.1–32.9)	-
Reader 2	0	61	0	25	-	-	23.0 (13.1–32.9)	-	23.0 (13.1–32.9)	-
Consensus	1	60	0	25	1.6 (0.0–4.8)	-	24.7 (14.7–34.6)	-	23.2 (13.3–33.1)	-
Nonenhancing capsule <sup>†</sup>										
Reader 1	0	75	0	29	-	-	22.5 (13.6–31.5)	-	22.5 (13.6–31.5)	-
Reader 2	0	75	0	29	-	-	22.5 (13.6–31.5)	-	22.5 (13.6–31.5)	-
Consensus	0	75	0	29	-	-	22.5 (13.6–31.5)	-	22.5 (13.6–31.5)	-
Nodule-in-nodule <sup>†</sup>										
Reader 1	1	74	0	29	1.3 (0.0–4.0)	-	24.2 (15.0–33.4)	-	22.9 (13.9–32.0)	-
Reader 2	0	75	0	29	-	-	22.5 (13.6–31.5)	-	22.5 (13.6–31.5)	-
Consensus	1	74	0	29	1.3 (0.0–4.0)	-	24.2 (15.0–33.4)	-	22.9 (13.9–32.0)	-
Mosaic architecture <sup>†</sup>										
Reader 1	6	69	0	29	7.9 (1.9–14.0)	-	30.7 (21.1–40.4)	-	24.5 (15.1–34.0)	-
Reader 2	7	68	0	29	9.3 (2.8–15.9)	-	31.6 (21.8–41.5)	-	24.9 (15.3–34.4)	-
Consensus	5	70	0	29	6.8 (1.0–12.6)	-	29.6 (19.8–39.4)	-	24.4 (15.0–33.9)	-
Blood products in mass <sup>†</sup>										
Reader 1	0	45	0	20	-	-	23.8 (11.8–35.8)	-	23.8 (11.8–35.8)	-
Reader 2	0	45	0	20	-	-	23.8 (11.8–35.8)	-	23.8 (11.8–35.8)	-
Consensus	0	45	0	20	-	-	23.8 (11.8–35.8)	-	23.8 (11.8–35.8)	-
Fat in mass more than adjacent liver <sup>†</sup>										
Reader 1	9	61	0	29	14.2 (4.4–23.9)	-	36.2 (25.6–46.8)	-	28.0 (17.8–38.3)	-
Reader 2	13	57	1	28	19.2 (8.8–29.5)	96.4 (89.2–100.0)	39.7 (29.3–50.1)	92.6 (78.4–100.0)	28.1 (17.7–38.6)	4.70 (0.62–35.54)
Consensus	10	60	1	20	15.1 (5.4–24.9)	96.4 (89.2–100.0)	35.7 (25.1–46.3)	90.3 (71.9–100.0)	26.9 (16.7–37.2)	3.73 (0.37–38.07)

Data in parentheses are 95% confidence intervals. Estimates of diagnostic performance were calculated with a generalized estimating equation (GEE) model to account for patient cluster effect. Dashes indicate that imaging feature was not evaluated by readers or that estimates of diagnostic performance could not be computed with GEE model because of small number of observations displaying this ancillary feature. Subthreshold growth was based on bookmarked measurements  
<sup>FN</sup> false-negative; <sup>FP</sup> false-positive; <sup>TN</sup> true-negative; <sup>TP</sup> true-positive  
<sup>†</sup>Features favoring hepatocellular carcinoma in particular as opposed to malignancy in general

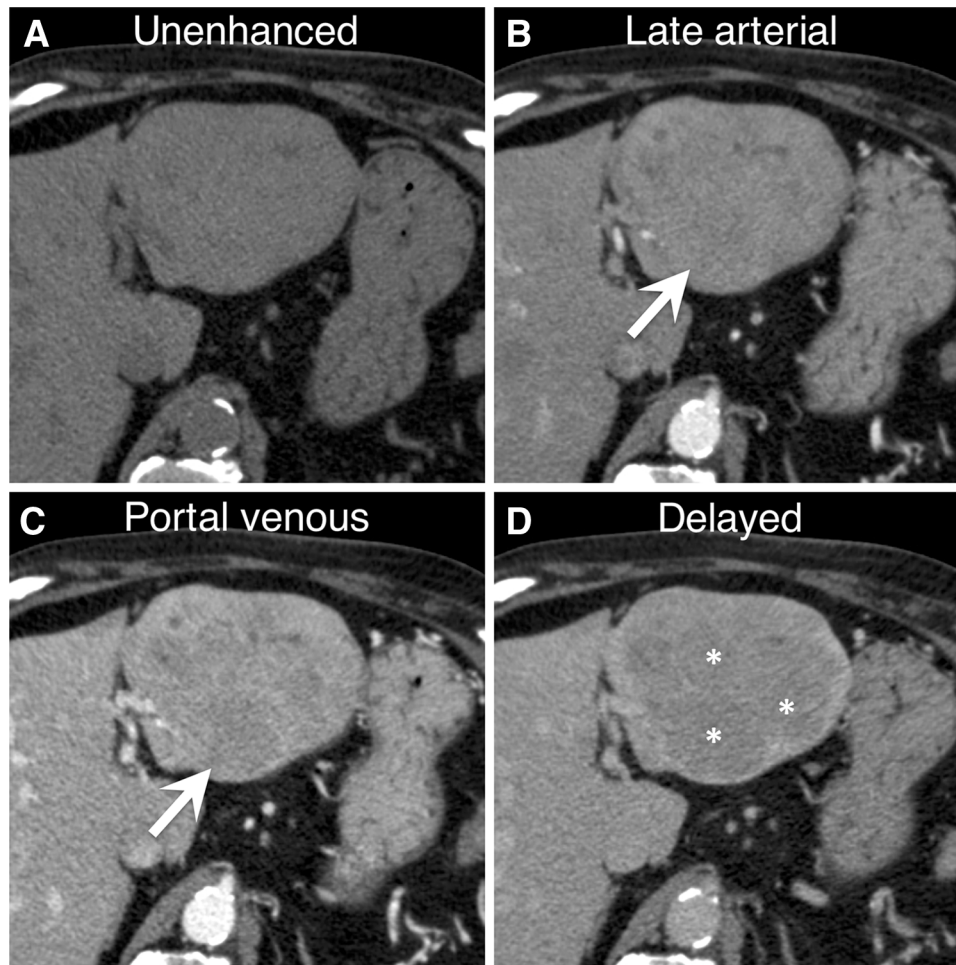


**Fig. 2.** Axial CT images in an 81-year-old man with cirrhosis and an 11-cm liver mass in segments II and III. **A** Images obtained before and after contrast enhancement in **(B)** late arterial phase shows arterial phase hyperenhancement (arrow) of the observation, **C** portal venous, and **D** delayed

phases shows washout appearance (arrow) and mosaic architecture (\*) of the mass. Observation was categorized LR-5 according to major features and hepatocellular carcinoma diagnosis was confirmed by pathology after hepatectomy.

Out of the 27 observations categorized LR-4 based on major features, 13 cases could not be upgraded to LR-5 (to respect the LI-RADS rule that a LR-4 observation cannot be upgraded to LR-5) and remained LR-4 despite the presence of subthreshold growth (7), US visibility as discrete nodule (9), corona enhancement (1), fat sparing in solid mass (1), and fat in mass, more than liver (2).

#### *Inter-reader agreement*

Supplementary Table 4 summarizes interreader kappa and observed agreement for major features, ancillary features, and LI-RADS categories. Agreement was not calculated for diameter, threshold growth, ultrasound visibility as discrete nodule, and subthreshold growth because those were bookmarked by the author and provided to both readers during reading sessions. Kappa

and observed agreement could not be calculated for fat sparing in solid mass, non-enhancing capsule, nodule-in-nodule, and blood product in mass because of perfect agreement.

Inter-reader agreement for major features was high for arterial phase hyperenhancement ( $\kappa = 0.90$ , proportion of observed agreement = 0.97) and washout ( $\kappa = 0.93$ , proportion of observed agreement = 0.97). Agreement was substantial for capsule ( $\kappa = 0.66$ , proportion of observed agreement = 0.89). Inter-reader agreement for ancillary features was fair to substantial ( $\kappa = 0.66$ –0.85, proportion of observed agreement = 0.93–0.99). Inter-reader agreement was high for LI-RADS categories assigned based on major features only ( $\kappa = 0.88$ , proportion of observed agreement = 0.91), and when assigned according to major

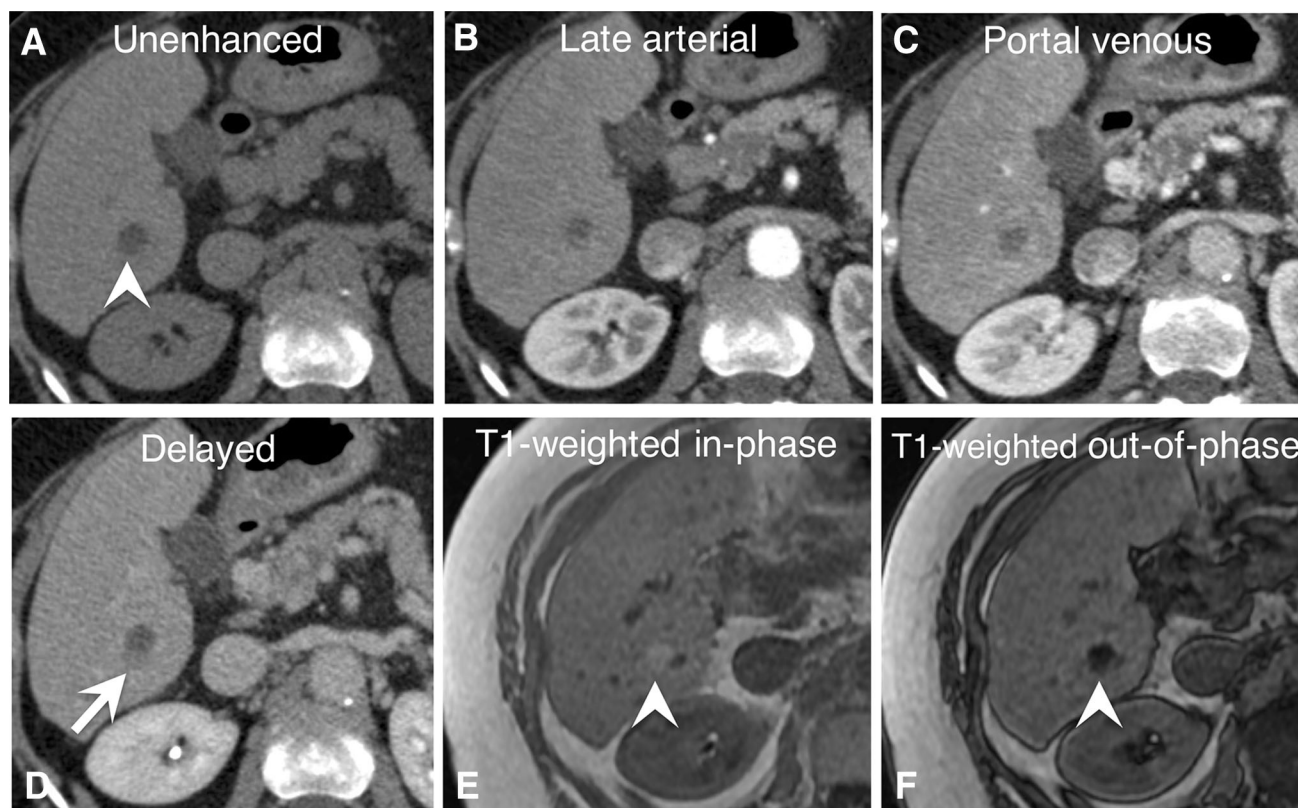


**Fig. 3.** Axial CT and MR images in a 76-year-old man with cirrhosis and an 18-mm liver observation in segment VI. **A** Axial CT images obtained before and after contrast administration in **(B)** late arterial, **(C)** portal venous, and **(D)** delayed phases shows intra-lesional fat (arrowhead), and subtle washout appearance at the posterior part of the mass (arrow). The observation was categorized LR-3 according to

major features, and upgraded to LR-4 category based on the presence of fat in mass, more than adjacent liver which is an ancillary feature in favor of malignancy. **E** Axial MRI gradient-recalled echo images in-phase, and **F** out-of-phase confirmed fat content by signal drop on out-of-phase imaging (arrowheads). Hepatocellular carcinoma diagnosis was confirmed by pathology after biopsy.

features in combination with ancillary features ( $\kappa = 0.90$ , proportion of observed agreement = 0.92).

## Discussion

For major features, we confirmed that larger observation diameter is a predictor for HCC diagnosis as described in prior studies with different size stratification thresholds [11, 19, 20]. However, the specificity for observation diameter  $\geq 10$  mm and  $\geq 20$  mm was lower than the pooled specificity of 86%–90% for observation diameter 10–20 mm and diameter  $> 20$  mm reported in the meta-analysis by Chou et al [16]. Although the high sensitivity of arterial phase hyperenhancement was within the range previously reported in the literature (65%–87%) [21–23], the specificity was lower than previously reported (81%) on CT by Sangiovanni et al [23] for  $\leq 1$  cm observations detected during ultrasound surveillance in patients with cirrhosis. This may be explained by the inclusion of non-ultrasound-detected observations in our study. Wash-out appearance as a standalone feature had a higher sensitivity, but lower specificity than previously reported [23].

The combination of arterial phase hyperenhancement and washout—a criteria used in other systems for the diagnosis of HCC [5, 8, 24]—provided a specificity within the range (66%–100%) reported in the literature [23, 25–27]. In our cohort, enhancing capsule has the highest specificity for the diagnosis of HCC, within the range (86%–96%) reported in previous MRI studies [28, 29].

Few studies have assessed the accuracy of ancillary features on CT, alone or in combination with major features, for diagnosis of HCC [13]. Among ancillary features favoring malignancy in general or HCC in particular, subthreshold growth and ultrasound visibility as discrete nodule had the highest sensitivity, whereas fat in mass more than adjacent liver had the highest specificity. Diagnostic performance could not be computed for corona enhancement, fat sparing in solid mass, non-enhancing capsule, nodule-in-nodule, mosaic architecture and blood product in mass because these features were rarely or never seen in our cohort. This is in line with a recent observation by Fowler et al that ancillary features were less commonly observed on CT than on MRI (26%

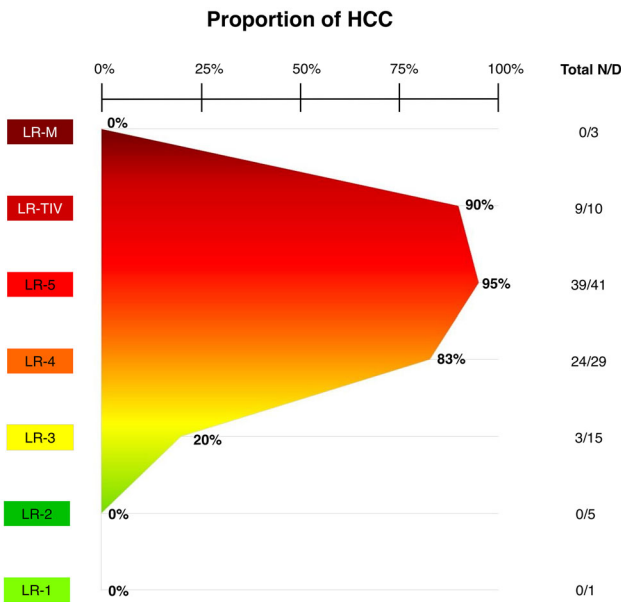


Fig. 4. Graphic illustrating the proportion of hepatocellular carcinomas for each LI-RADS category. *HCC* hepatocellular carcinoma. *N* nominator, *D* denominator.

	LR-M	LR-TIV	LR-5	LR-4	LR-3	LR-2	LR-1	
Major and Ancillary Features	3 (2.9%)	9 (8.7%)	42 (40.4%)	29 (26.0%)	15 (14.4%)	5 (2.9%)	1 (1.0%)	3
Major Features Only	N/A	N/A	42 (40.4%)	27 (26.0%)	15 (14.4%)	3 (2.9%)	1 (1.0%)	3
	N/A	N/A	N/A	2 (1.9%)	0	0	0	19
	N/A	N/A	N/A	NA	0	2 (1.9%)	NA	27
	N/A	N/A	NA	NA	NA	NA	NA	42
	N/A	9 (8.7%)	N/A	NA	NA	NA	N/A	9
	3 (2.9%)	N/A	N/A	NA	NA	N/A	N/A	3

Fig. 5. Diagram shows numbers and percentages of observation before and after application of ancillary features according to Liver Imaging Reporting and Data System (LI-RADS) version 2017 application rules. Color coding of each LI-RADS category is identical to color convention used in official LI-RADS documents. N/A indicates category changes that are not permitted by LI-RADS version 2017 rules [3].

and 74% respectively) [9]. Ultrasound visibility as discrete nodule, which is an ancillary feature added in the updated version of LI-RADS v2017, was the most frequently encountered feature with 27 observations seen on US, 24 of which were HCCs. In contrast, non-enhancing

capsule which is also a new ancillary feature favoring HCC in particular in the 2017 version of LI-RADS was never encountered in our study. A subtype of non-enhancing capsule has been described in the literature as a small hypointense rim on hepato-biliary phase MRI but seldom described on CT [30–32].

The present study confirms the high specificity and positive predictive value of LI-RADS categories LR-5 and LR-TIV for the diagnosis of HCC. Our results are similar to those reported by Ronot et al who reported a specificity of 88.3% and a positive predictive value of 90.9% for the LR-5 and LR-5V combination based on LI-RADS v2014 [13]. Combining the LR-4, LR-5, and LR-TIV categories increases the sensitivity but with a decrease in specificity. The combination of (LR-4, LR-5 and LR-TIV) categories for the diagnosis of HCC remains controversial in the literature. Ronot et al. reported an increase in sensitivity (from 69.6% to 85.8%), and a significant decrease in specificity (from 88.3% to 66.0%) similar to our results. Others reported a marked increase in sensitivity with no loss in specificity, but those were limited to MRI [33, 34]. Application of ancillary features provided similar sensitivity and specificity for individual categories (e.g., LR-3 or LR-4) or combinations of categories (e.g., LR-4, LR-5, and LR-TIV). This may be explained by the LI-RADS v2017 application rules that specify that category upgrade or downgrade is optional, at the discretion of radiologists.

For major features, inter-reader agreement was substantial to almost perfect, highest for washout followed by arterial phase hyperenhancement, both higher than previously reported ( $\kappa = 0.61–0.84$  and  $0.54–0.86$ , respectively) in the literature [9, 12, 34–36]. This could be explained by the fact that our study was limited to CT and both readers had similar experience. For ancillary features, agreement was high for corona enhancement, substantial for intra-lesional fat and moderate for mosaic architecture. Kappa could not be calculated for fat sparing in solid mass, non-enhancing capsule and blood product in mass because of perfect agreement. For LI-RADS categories, agreement was almost perfect before and after applying ancillary features.

Our study had some limitations. First, it was a retrospective study so selection bias may affect generalizability. However, selection criteria were defined to respect LI-RADS technical requirements, the referral pattern at our tertiary care center, and the requirement for a reference standard. Second, the exclusion criteria—which were required to exclude patients with a known history of HCC, technically inadequate examinations such as unenhanced CT, and absence of contemporaneous reference standard—decreased the patient sample size. Nevertheless, the per-lesion unit of analysis included 104 observations, a sample size similar to that of prior diagnostic CT studies [23, 25–27, 37]. Fourth, the application of ancillary features to adjust the observation

category was left at the discretion of radiologists, as stated in the LI-RADS application rules for ancillary features. Hence, decisions to adjust observation category were subjective. Future research studying the thought process leading to category adjustment is needed. Finally, the reference standard for the final diagnosis of HCC not based on a histopathological diagnosis alone but on a composite reference standard. Restricting our eligibility criteria to patients with pathologically confirmed specimens only would have introduced a confirmation bias. This approach is congruent with current clinical guidelines that do not mandate pathological proof for observations that meet diagnostic imaging criteria.

In conclusion, our CT study confirms that LI-RADS major features have moderate to excellent specificity and LR-5 category has a near-perfect specificity for the diagnosis of HCC. Use of ancillary features on CT at the discretion of the radiologist modifies the final category in a small number of cases, but provides similar sensitivity and specificity for the diagnosis of HCC. Combining the LR-4, LR-5, and LR-TIV categories increases the sensitivity but with a decrease in specificity. Interreader agreement was substantial to almost perfect for major features, moderate to almost perfect for ancillary features, and almost perfect for categories.

#### Compliance with ethical standards

**Conflict of interest** Ayman Alhasan, Milena Cerny, Damien Olivie, Jean-Sébastien Billiard, Catherine Bergeron, Kip Brown, Paule Bodson-Clermont, Hélène Castel, Simon Turcotte, Pierre Perreault and An Tang declare that they have no conflict of interest.

**Ethical approval** All procedures performed in studies involving human participants were in accordance with the ethical standards of the institutional and/or national research committee and with the 1964 Helsinki declaration and its later amendments or comparable ethical standards.

**Informed consent** Informed consent was waived from all individual participants included in the study.

#### References

- Mittal S, El-Serag HB (2013) Epidemiology of hepatocellular carcinoma: consider the population. *J Clin Gastroenterol* 47(Suppl):S2–S6. <https://doi.org/10.1097/MCG.0b013e3182872f29>
- Omata M, Lesmana LA, Tateishi R, et al. (2010) Asian Pacific Association for the Study of the Liver consensus recommendations on hepatocellular carcinoma. *Hepatology* 42(2):439–474. <https://doi.org/10.1007/s12072-010-9165-7>
- American College of Radiology. (2018) Liver Imaging Reporting and Data System (LI-RADS) version 2017. <https://www.acr.org/Clinical-Resources/Reporting-and-Data-Systems/LI-RADS>. Accessed April 20, 2018
- Heimbach JK, Kulik LM, Finn RS, et al. (2018) AASLD guidelines for the treatment of hepatocellular carcinoma. *Hepatology* 67(1):358–380. <https://doi.org/10.1002/hep.29086>
- European Association for the Study of the Liver. Electronic address eee, European Association for the Study of the L (2018) EASL clinical practice guidelines: management of hepatocellular carcinoma. *J Hepatol* . <https://doi.org/10.1016/j.jhep.2018.03.019>
- Elsayes KM, Hooker JC, Agrons MM, et al. (2017) 2017 version of LI-RADS for CT and MR imaging: an update. *Radiographics* 37(7):1994–2017. <https://doi.org/10.1148/rg.2017170098>
- Tang A, Bashir MR, Corwin MT, et al. (2018) Evidence supporting LI-RADS major features for CT- and MR imaging-based diagnosis of hepatocellular carcinoma: a systematic review. *Radiology* 286(1):29–48. <https://doi.org/10.1148/radiol.2017170554>
- Organ Procurement and Transplantation Network. (2018) OPTN/UNOS policy 9: allocation of livers and liver-intestines. [https://optn.transplant.hrsa.gov/media/1200/optn\\_policies.pdf](https://optn.transplant.hrsa.gov/media/1200/optn_policies.pdf). Accessed April 20, 2018
- Fowler KJ, Tang A, Santillan C, et al. (2018) Interreader reliability of LI-RADS version 2014 algorithm and imaging features for diagnosis of hepatocellular carcinoma: a large international multi-reader study. *Radiology* 286(1):173–185. <https://doi.org/10.1148/radiol.2017170376>
- Fraum TJ, Tsai R, Rohe E, et al. (2018) Differentiation of hepatocellular carcinoma from other hepatic malignancies in patients at risk: diagnostic performance of the liver imaging reporting and data system version 2014. *Radiology* 286(1):158–172. <https://doi.org/10.1148/radiol.2017170114>
- Cerny M, Bergeron C, Billiard JS, Murphy-Lavallee J, Olivie D, Berube J, Fan B, Castel H, Turcotte S, Perreault P, Chagnon M, Tang A (2018) LI-RADS for MR imaging diagnosis of hepatocellular carcinoma: performance of major and ancillary features. *Radiology*. <https://doi.org/10.1148/radiol.2018171678>
- Joo I, Lee JM, Lee DH, et al. (2017) Liver imaging reporting and data system v2014 categorization of hepatocellular carcinoma on gadoteric acid-enhanced MRI: comparison with multiphase multidetector computed tomography. *J Magn Reson Imaging* 45(3):731–740. <https://doi.org/10.1002/jmri.25406>
- Ronot M, Fouque O, Esvan M, et al. (2017) Comparison of the accuracy of AASLD and LI-RADS criteria for the non-invasive diagnosis of HCC smaller than 3 cm. *J Hepatol* . <https://doi.org/10.1016/j.jhep.2017.12.014>
- Choi JY, Lee JM, Sirlin CB (2014) CT and MR imaging diagnosis and staging of hepatocellular carcinoma: part II. Extracellular agents, hepatobiliary agents, and ancillary imaging features. *Radiology* 273(1):30–50. <https://doi.org/10.1148/radiol.14132362>
- Lee JM, Yoon JH, Joo I, Woo HS (2012) Recent advances in CT and MR imaging for evaluation of hepatocellular carcinoma. *Liver Cancer* 1(1):22–40. <https://doi.org/10.1159/000339018>
- Chou R, Cuevas C, Fu R, et al. (2015) Imaging techniques for the diagnosis of hepatocellular carcinoma: a systematic review and meta-analysis. *Ann Intern Med* 162(10):697–711. <https://doi.org/10.7326/M14-2509>
- Hanna RF, Miloushev VZ, Tang A, et al. (2016) Comparative 13-year meta-analysis of the sensitivity and positive predictive value of ultrasound, CT, and MRI for detecting hepatocellular carcinoma. *Abdom Imaging*. 41(1):71–90. <https://doi.org/10.1007/s00261-015-0592-8>
- Landis JR, Koch GG (1977) The measurement of observer agreement for categorical data. *Biometrics* 33(1):159–174
- Bolondi L, Gaiani S, Celli N, et al. (2005) Characterization of small nodules in cirrhosis by assessment of vascularity: the problem of hypovascular hepatocellular carcinoma. *Hepatology* 42(1):27–34. <https://doi.org/10.1002/hep.20728>
- Forner A, Vilana R, Ayuso C, et al. (2008) Diagnosis of hepatic nodules 20 mm or smaller in cirrhosis: prospective validation of the noninvasive diagnostic criteria for hepatocellular carcinoma. *Hepatology* 47(1):97–104. <https://doi.org/10.1002/hep.21966>
- Oliver JH 3rd, Baron RL, Federle MP, Rockette HE Jr (1996) Detecting hepatocellular carcinoma: value of unenhanced or arterial phase CT imaging or both used in conjunction with conventional portal venous phase contrast-enhanced CT imaging. *AJR Am J Roentgenol* 167(1):71–77. <https://doi.org/10.2214/ajr.167.1.8659425>
- Laghi A, Iannaccone R, Rossi P, et al. (2003) Hepatocellular carcinoma: detection with triple-phase multi-detector row helical CT in patients with chronic hepatitis. *Radiology* 226(2):543–549. <https://doi.org/10.1148/radiol.2262012043>
- Sangiovanni A, Manini MA, Iavarone M, et al. (2010) The diagnostic and economic impact of contrast imaging techniques in the

- diagnosis of small hepatocellular carcinoma in cirrhosis. *Gut* 59(5):638–644. <https://doi.org/10.1136/gut.2009.187286>
24. Bruix J, Reig M, Rimola J, et al. (2011) Clinical decision making and research in hepatocellular carcinoma: pivotal role of imaging techniques. *Hepatology* 54(6):2238–2244. <https://doi.org/10.1002/hep.24670>
  25. Burrel M, Llovet JM, Ayuso C, et al. (2003) MRI angiography is superior to helical CT for detection of HCC prior to liver transplantation: an explant correlation. *Hepatology* 38(4):1034–1042. <https://doi.org/10.1053/jhep.2003.50409>
  26. Serste T, Barrau V, Ozenne V, et al. (2012) Accuracy and disagreement of computed tomography and magnetic resonance imaging for the diagnosis of small hepatocellular carcinoma and dysplastic nodules: role of biopsy. *Hepatology* 55(3):800–806. <https://doi.org/10.1002/hep.24746>
  27. Jang HJ, Kim TK, Khalili K, et al. (2013) Characterization of 1-to 2-cm liver nodules detected on hcc surveillance ultrasound according to the criteria of the American Association for the Study of Liver Disease: is quadruphasic CT necessary? *AJR Am J Roentgenol* 201(2):314–321. <https://doi.org/10.2214/AJR.12.9341>
  28. Khan AS, Hussain HK, Johnson TD, et al. (2010) Value of delayed hypointensity and delayed enhancing rim in magnetic resonance imaging diagnosis of small hepatocellular carcinoma in the cirrhotic liver. *J Magn Reson Imaging* 32(2):360–366. <https://doi.org/10.1002/jmri.22271>
  29. Rimola J, Forner A, Tremosini S, et al. (2012) Non-invasive diagnosis of hepatocellular carcinoma  $\leq$  2 cm in cirrhosis. Diagnostic accuracy assessing fat, capsule and signal intensity at dynamic MRI. *J Hepatol* 56(6):1317–1323. <https://doi.org/10.1016/j.jhep.2012.01.004>
  30. An C, Park MS, Kim D, et al. (2013) Added value of subtraction imaging in detecting arterial enhancement in small (< 3 cm) hepatic nodules on dynamic contrast-enhanced MRI in patients at high risk of hepatocellular carcinoma. *Eur Radiol* 23(4):924–930. <https://doi.org/10.1007/s00330-012-2685-x>
  31. Suh YJ, Kim MJ, Choi JY, et al. (2011) Differentiation of hepatic hyperintense lesions seen on gadoxetic acid-enhanced hepatobiliary phase MRI. *AJR Am J Roentgenol* 197(1):W44–W52. <https://doi.org/10.2214/ajr.10.5845>
  32. Dioguardi Burgio M, Picone D, Cabibbo G, et al. (2016) MR-imaging features of hepatocellular carcinoma capsule appearance in cirrhotic liver: comparison of gadoxetic acid and gadobenate dimeglumine. *Abdom Radiol (NY)* 41(8):1546–1554. <https://doi.org/10.1007/s00261-016-0726-7>
  33. Darnell A, Forner A, Rimola J, et al. (2015) Liver Imaging Reporting and Data System with MR Imaging: evaluation in Nodules 20 mm or smaller detected in cirrhosis at screening US. *Radiology* 275(3):698–707. <https://doi.org/10.1148/radiol.15141132>
  34. Zhang YD, Zhu FP, Xu X, et al. (2016) Classifying CT/MR findings in patients with suspicion of hepatocellular carcinoma: comparison of liver imaging reporting and data system and criteria-free Likert scale reporting models. *J Magn Reson Imaging* 43(2):373–383. <https://doi.org/10.1002/jmri.24987>
  35. Ehman EC, Behr SC, Umetsu SE, et al. (2016) Rate of observation and inter-observer agreement for LI-RADS major features at CT and MRI in 184 pathology proven hepatocellular carcinomas. *Abdom Radiol (NY)* 41(5):963–969. <https://doi.org/10.1007/s00261-015-0623-5>
  36. Bashir MR, Huang R, Mayes N, et al. (2015) Concordance of hypervascular liver nodule characterization between the organ procurement and transplant network and liver imaging reporting and data system classifications. *J Magn Reson Imaging* 42(2):305–314. <https://doi.org/10.1002/jmri.24793>
  37. Denecke T, Grieser C, Froling V, et al. (2009) Multislice computed tomography using a triple-phase contrast protocol for preoperative assessment of hepatic tumor load in patients with hepatocellular carcinoma before liver transplantation. *Transpl Int* 22(4):395–402. <https://doi.org/10.1111/j.1432-2277.2008.00793.x>